NANO LETTERS
Letter
Cite This: Nano Lett. 2019, 19, 6027−6034
pubs.acs.org/NanoLett

Photoexcitation Induced Quantum Dynamics of Charge Density Wave and Emergence of a Collective Mode in 1*T*-TaS_2

Jin Zhang,[†,‡,¶] Chao Lian,[†,¶] Mengxue Guan,[†,‡,¶] Wei Ma,[†,‡] Huixia Fu,[†,‡] Haizhong Guo,[§] and Sheng Meng*[,†,‡,⊥]

[†]Beijing National Laboratory for Condensed Matter Physics, Institute of Physics, Chinese Academy of Sciences, Beijing 100190, P. R. China
[‡]School of Physical Sciences, University of Chinese Academy of Sciences, Beijing 100049, P. R. China
[§]School of Physics and Engineering, Zhengzhou University, Zhengzhou, Henan 450001, P. R. China
[⊥]Songshan Lake Materials Laboratory, Dongguan, Guangdong 523808, P. R. China

Supporting Information

ABSTRACT: Photoexcitation is a powerful means in distinguishing different interactions and manipulating the states of matter, especially in charge density wave (CDW) materials. The CDW state of 1*T*-TaS_2 has been widely studied experimentally mainly because of its intriguing laser-induced ultrafast responses of electronic and lattice subsystems. However, the microscopic atomic dynamics and underlying electronic mechanism upon photoexcitation remain unclear. Here, we demonstrate photoexcitation induced ultrafast dynamics of CDW in 1*T*-TaS_2 using time-dependent density functional theory molecular dynamics. We discover a novel collective oscillation mode between the CDW state and a transient state induced by photodoping, which is significantly different from thermally induced phonon mode and attributed to the modification of the potential energy surface from laser excitation. In addition, our finding validates nonthermal melting of CDW induced at low light intensities, supporting that conventional hot electron model is inadequate to explain photoinduced dynamics. Our results provide a deep insight into the coherent electron and lattice quantum dynamics during the formation and excitation of CDW in 1*T*-TaS_2.

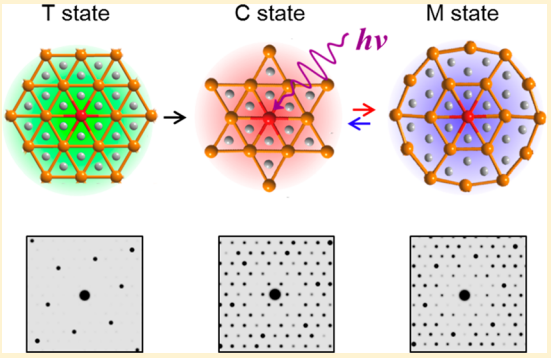

KEYWORDS: *charge density wave, TDDFT, photoinduced phase transition, nonthermal melting, nonadiabatic dynamics*

Interplay among different degrees of freedom including electrons, phonons, and spins is of paramount importance in understanding and optimizing the properties of quantum materials.[1−3] Optical excitation is a powerful tool to distinguish different interactions and to manipulate the state of matter. Furthermore, dominant interactions can be identified, and meaningful insights into ground-state properties, phase transitions, and hidden phases can be obtained.[4−8] It is particularly useful for complex quantum systems, where a variety of degrees of freedom and quantum interactions coexist and are strongly coupled.

A particular example would be charge density wave (CDW) materials.[9−16] The layered transition-metal dichalcogenides such as 1*T*-TaS_2 have been widely investigated to understand CDW physics in real materials.[17−40] 1*T*-TaS_2 is a typical quasi two-dimensional CDW material with a pristine lattice constant of 3.36 Å in undistorted 1*T* phase (referred to as *T* state). The canonical origin of CDW phase is usually attributed to the Fermi-surface nesting, driven by electron−phonon coupling via the Peierls mechanism.[31−35] In the low-temperature commensurate CDW phase, referred to as C state hereafter, 1*T*-TaS_2 becomes strongly modulated, leading to a lattice distortion with a new periodicity of ∼12.1 Å rotated by 13.9°. Charge transfer from the outer ring toward the center results in the famous pattern, namely the "star of David" (SD) shape of the lattice distribution.

Laser-induced phase dynamics in 1*T*-TaS_2 has been widely investigated experimentally in recent years.[17,21−26] Excitation with ultrashort laser pulses closes both CDW and Mott gaps in 1*T*-TaS_2. At low intensities, it also excites the breathing phonon mode (the amplitude mode of the CDW), where the atomic clusters and the charge order oscillate synchronously around the equilibrium state.[21−23,25−30] The ultrafast melting of Mott gap upon strong laser excitation has been observed, while the lattice retains its low-temperature symmetry.[22] However, it is not definitely clear whether the lattice degree of freedom and ionic movements are simultaneously coupled to electronic modulations and the underlying mechanism of photoexcitation under extreme conditions.[21−23]

Received: May 7, 2019
Revised: August 8, 2019
Published: August 16, 2019

DOI: 10.1021/acs.nanolett.9b01865
Nano Lett. 2019, 19, 6027−6034

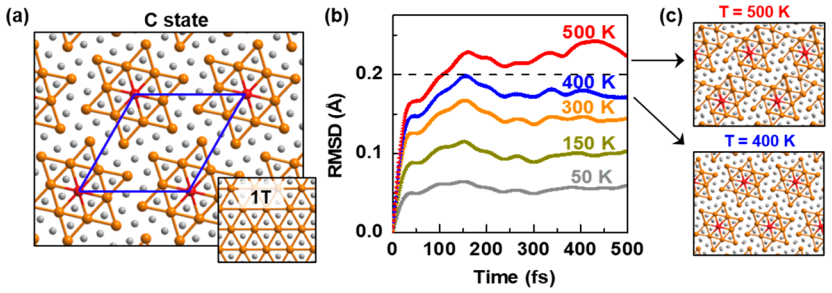

Figure 1. Charge density wave state of bulk 1*T*-TaS_2 and its thermal melting. (a) Atomic structure of 1*T*-TaS_2 in C state with a $\sqrt{13} \times \sqrt{13}$ superlattice (blue rhombus). Inset shows the undistorted 1T phase of bulk TaS_2. (b) Root−mean−square displacement (RMSD) of 1*T*-TaS_2 under different ionic temperatures from Born−Oppenheimer molecular dynamics (BOMD) simulations. (c) Snapshots of the structures at 500 fs of BOMD at 400 K (lower panel) and 500 K (upper panel). The dashed line indicates the critical value for the destruction of periodically modulated structures. Orange and gray spheres denote Ta and S atoms, respectively, and red spheres are Ta atoms at the center of stars. The criterion for making Ta−Ta bonds is that the Ta−Ta distance is shorter than 3.4 Å.

To explain phase dynamics of 1*T*-TaS_2 under laser illumination, the hot electron model was widely invoked to understand the interactions between electron and lattice subsystem.[17,21,22] In such a model, the excited electrons rapidly thermalize among themselves forming hot electron gas with a given electronic temperature (T_e) of several thousands of Kelvin, significantly higher than that of the lattice subsystem. The cold lattice is then heated up by hot electrons via effective electron−phonon interactions. The melting of CDW state and bandgap closing takes place when the lattice temperature is higher than its equilibrium thermal melting temperature. Here, "Gap closing" indicates the collapse of the electronic gap, attributed to the melting of the charge order in 1*T*-TaS_2.[17,21] Nevertheless, it conflicts with the fact that excited electrons and the lattice take a quite long time (>1 ps) to reach equilibrium with a Fermi−Dirac electronic distribution,[35] while an ultrafast (∼30 fs) band gap closing was observed in the recent experimental measurement.[22] Another picture is that phase dynamics is induced by the modification of the potential energy surfaces. Strong lasers and ultrafast electron−electron scattering strongly modify the potential energy surface. It may lead to cooperative atomic motions toward a new photoinduced phase, which largely resembles the symmetric undistorted 1*T* phase.[21] However, the microscopic atomic dynamics and underlying mechanism for 1*T*-TaS_2 under laser excitation are still under debate.

In this work, we investigate the atomistic mechanism and ultrafast photoinduced dynamics of CDW in 1*T*-TaS_2, using nonadiabatic molecular dynamics (MD) simulations based on time-dependent density functional theory (TDDFT). Our first-principles simulations provide for the first time intrinsic electron-nuclei coupled dynamics of 1*T*-TaS_2 (Note S1).[41−48] Amplitude mode and nonthermal melting of CDW are successfully reproduced at low laser intensities. At higher laser intensity, a laser-induced new collective mode appears, with distinctive electronic properties. We study the CDW physics and the interactions between multiple degrees of freedom therein from the perspective of ultrafast phase dynamics of 1*T*-TaS_2 under photoexcitation. We find that the widely accepted hot electron model is inadequate to account for dynamic phenomena observed in experiments because of the lack of electron−electron scattering effect. This work not only gives a deep insight into the photoinduced nonequilibrium dynamics of 1*T*-TaS_2 but also provides a framework to understand laser-induced phenomena in more complex quantum materials.

At high temperatures, 1*T*-TaS_2 is metallic, exhibiting an undistorted lattice. Below 350 K, the SD shaped patterns of tantalum atoms show up, accompanied by a periodical lattice distortion. At temperatures below 180 K, the CDW state brings an insulating electronic structure due to the presence of a fully commensurate CDW with the long-ranged $\sqrt{13} \times \sqrt{13}$ superlattice.[20] Figure 1a shows the atomic structure of 1*T*-TaS_2 in its ground-state C phase with the SD pattern, which is energetically favored over the *T* phase (by 73 meV/atom). An in-plane band gap of 0.45 eV in the CDW state of TaS_2 is induced by periodical lattice distortions, consistent with previous experimental and theoretical studies.[21,49,50]

We focus on the dynamics of CDW phase under different thermal and laser conditions. To demonstrate the behavior of bulk 1*T*-TaS_2 under different temperatures, root−mean−square displacement (RMSD = $\sqrt{u^2(t)}$, where $u(t)$ is the atomic displacement of all atoms relative to the ground-state C state) is recorded to quantify the lattice structural changes. Figure 1b shows the evolution of RMSD under different ionic temperatures in Born−Oppenheimer molecular dynamics (BOMD). The equilibrium value of RMSD increases as the ionic temperature rises. We find that the critical point to melt CDW state is located at ∼400 K, when the RMSD reaches 0.2 Å. The CDW pattern observed in experiments is distorted by 7% from the symmetric 1T shape, which rationalizes the value obtained here, see Figure S1 in Supporting Information.[20] At this temperature, the ionic SDs start to disappear, and the lattice restores its undistorted 1*T* geometry where the spatial modulation becomes much weaker. Snapshots of atomic structures are presented in Figure 1c, and more details can be found in Figure S1. We adopt a criterion that the CDW state melts or transforms to a new phase when the RMSD value reaches R_c = 0.2 Å, based on the collapse temperature of the SDs. Thus, the CDW state in bulk 1*T*-TaS_2 melts thermally at about 400 K with a maximum RMSD of 0.2 Å in our simulations. The term "melting" indicates the destruction of the $\sqrt{13} \times \sqrt{13}$ CDW order in 1*T*-TaS_2 and creating an undistorted *T* state without reconstruction. The amplitude mode of the C state indicates the oscillations corresponding closely to the breathing mode of the stars, leading to the atomic collective oscillations rather than phase destruction. In contrast, atomic fluctuation or topological defects may introduce structural instability, resulting in phase transition like domain-like long-range ordered state.[51−55] The small deviation from the experimental value of 350 K may arise from

DOI: 10.1021/acs.nanolett.9b01865
Nano Lett. 2019, 19, 6027−6034

the supercell constraint of the model used. We note that the nearly commensurate and incommensurate CDW phases cannot be directly simulated because of periodic boundary conditions and small supercells used here.

We have shown the structural dynamics only considering the effect of the ionic temperature in Figure 1. In the following, we strive to understand the photoexcitation induced electronic and ionic dynamics under different laser intensities. To illustrate the laser-induced charge modulation in bulk 1*T*-TaS_2, we elaborately build initial states of photoexcitation. First, we use a Gaussian-envelope function $E(t)$ to describe the laser pulse applied:

$$E(t) = E_0 \cos(\omega t) \exp\left[-\frac{(t-t_0)^2}{2\sigma^2}\right] \quad (1)$$

Here, E_0, ω, t_0, and σ are maximum strength of the electric filed, the photon energy, the peak time of the electric field, and the width of the Gaussian pulse, respectively, as shown in Figure 2a. Previous work has shown that density functional theory can well describe the electronic structure and the optical properties of the bulk 1*T*-TaS_2.[49] The laser parameters are set to match to those of experimental references.[17,21,22] The photon energy 1.6 eV corresponds to the laser wavelength of ~800 nm, which is widely adopted in optical measurements.[21,22] The pulse broadening factor is set to gain comparable laser fluence with experimental data.[20] The electronic excitations as well as the atomic displacements can be tuned by modulating the laser intensity (Figures S2−S5). In addition, we have tested the dynamics using lasers with different in-plane polarizations, validating that the new vibrational mode is not dependent on the direction of the laser.

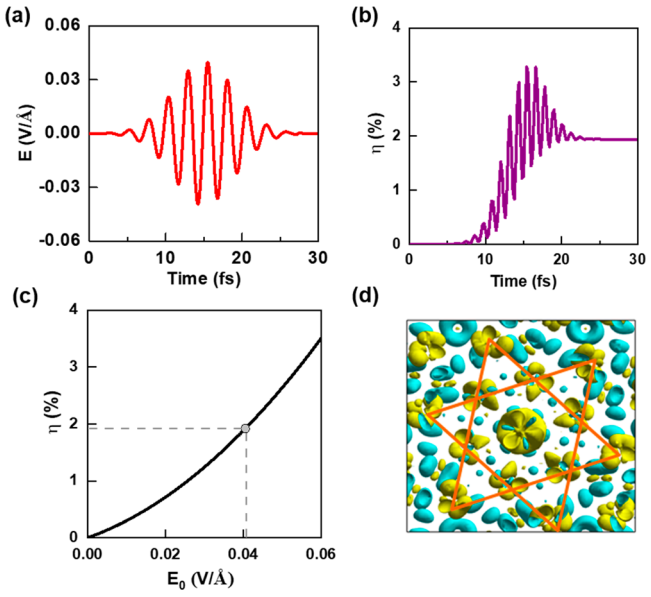

Figure 2. Laser-induced excited carriers of 1*T*-TaS_2. (a) Applied electric field along the in-plane direction of bulk 1*T*-TaS_2 with the laser strength E_0 = 0.041 V/Å. The pulse width is 4 fs, and the photon energy is 1.6 eV, respectively. The laser field value reaches the maximum strength E_0 at time t_0 = 15 fs. Similar few-cycle pulses have been widely applied experimentally to engineer electronic excitations and ultrafast dynamics in gases and solids. (b) Amount of excited electrons (η) upon photoexcitation from the valence bands to conduction bands under the laser pulse presented in panel a after the laser pulse. (c) Dependence of the percentage of excited electrons on laser strength E_0. The gray dot shows the photoexcitation condition as mentioned in panels a and b. (d) Laser pulses induced charge density redistribution when η = 1.92% at t = 25 fs. The yellow (light blue) region represents density increase (decrease) in charge density with the isosurface value of 0.05 e/Å^3 and the SDs are presented with orange lines.

Figure 2b illustrates the number of excited electrons from the valence bands to conduction bands upon laser excitation. The number of excited electrons first fluctuates with the laser field and then stabilizes after 20 fs when the laser field diminishes. The η value is used to denote the percentage of valence electrons pumped to conduction bands. For instance, η = 1% means that 1% of total valence electrons are pumped to specified unoccupied bands. The dependence of the number of excited electrons on laser strength E_0 is calculated by projecting the time-evolved wave functions ($|\psi_{n,k}(t)\rangle$) on the basis of the ground-state wave functions ($|\varphi_{n',k}\rangle$):

$$\eta(t) = \frac{1}{n_e}\frac{1}{N_k}\sum_{n,n'}^{CB}\sum_{k}^{BZ} |\psi_{n',k}(t)|\varphi_{n',k}|^2 \quad (2)$$

where N_k is the total number of the k-points used to sample the Brillouin zone, and n_e is the total number of electrons. The sum over the band indices n and n' run over all conduction bands and the maximum value of $\eta(t)$ is recorded.

We find that optical excitations bring about an increase in charge density near the center of the SD and a clear depletion around the edge of the stars, as shown in Figure 2d. For E_0 = 0.04 V/Å, the final η approaches 1.92%. With the growth of the laser strength E_0, the stable η value increases significantly, as shown in Figure 2c. When E_0 reaches 0.057 V/Å, η is as high as 3.20%. This builds a clear relationship between the laser intensity and the photoexcited electrons. For convenience, we use the percentage η of valence electrons pumped to conduction bands to denote the laser intensity.

We consider photoinduced ultrafast dynamics in 1*T*-TaS_2 under different laser intensities. At low laser intensity η = 0.64% (ca. 0.25 mJ/cm^2), atomic positions of 1*T*-TaS_2 change very little (Figure 3a). Here, we assume that about 10% of the laser energy is absorbed by the samples in real experiments. The RMSD increases to only 0.06 Å after about 200 fs and then stays stable at such a value (black line in Figure 3b). We note that a small modulation in RMSD shows up with a period of ~400 fs, corresponding to the amplitude mode of CDW.

For a stronger laser intensity η = 1.28% (ca. 0.50 mJ/cm^2), we observe phase destruction (melting) of the SD at ~250 fs after photoexcitation in Figure 3. The value of RMSD reaches a maximum (0.25 Å) at 440 fs and then stabilizes at this value, larger than the critical value of melting (R_c = 0.2 Å), implying that the CDW state melts. We monitor the corresponding lattice temperatures after the photoexcitation in Figure 3c and find the temperature grows from the initial temperature 10 to 103 K after 100 fs, attributed to the energy transfer from Kohn−Sham electronic orbitals to the kinetic energy of the lattice subsystem. This can be regarded as the time scale for excited electrons and holes transfer their excess energy to the lattice, that is, the time scale of electron−phonon coupling. The concurrent ionic temperature is evidently lower than that of thermal melting (~400 K), indicating that the ultrafast CDW melting is not originated from the higher lattice temperature without electronic excitation.

For an even stronger laser intensity of η = 1.92% (ca. 0.75 mJ/cm^2), laser-induced phase dynamics in bulk 1*T*-TaS_2 is also

DOI: 10.1021/acs.nanolett.9b01865
Nano Lett. 2019, 19, 6027−6034

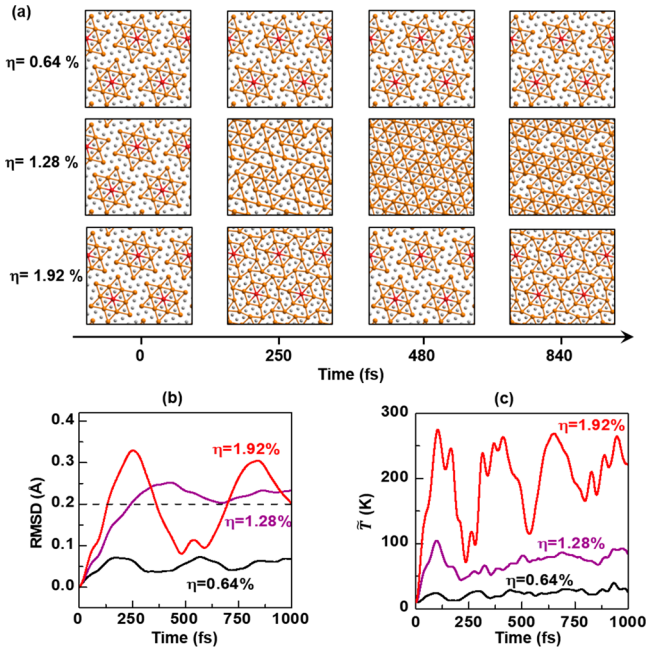

Figure 3. Time evolution of atomic structures of bulk 1*T*-TaS_2 under different photoexcitation. (a) Snapshots of time-dependent atomic structures for η = 0.64%, η = 1.28%, and η = 1.92% at 0, 250, 480, and 840 fs after photoexcitation, respectively. (b) Evolution of RMSD under three laser intensities (black line, η = 0.64%; purple line, η = 1.28%; red line, η = 1.92%). R_c is shown by a dashed black line. (c) Corresponding evolution of the ionic temperatures calculated from the kinetic energy of all ions at different times.

shown in Figure 3. Very surprisingly, the electron−nuclear dynamics is very distinctive from the above cases: not only the RMSD exhibits a periodical oscillation with a time period of 480 fs but also a new photoinduced transient metallic state (referred to as M state) with spatially ordered atomic structures is obtained. Eventually, the maximum of RMSD reaches 0.32 Å at 250 fs in Figure 3b, where the SD collapses evidently and a new order is generated. After that, the value of RMSD decreases to 0.1 Å below R_c and the atomic structure resembles that in C state, which is fully restored at t = 480 fs. In the meantime, the corresponding ionic temperature grows to 270 K within 110 fs and then oscillates around 200 K (Figure 3c). For stronger laser intensity of η = 3.2%, the features of charge-lattice dynamics are similar, despite that the lattice temperature reaches above 400 K (Figure S6). The photoinduced transient state also appears at 210 fs with a maximum RMSD of 0.35 Å. Therefore, a laser with stronger intensity will not change the charge-lattice correlated dynamics, except that the ionic temperature of the system increases to ∼400 K. In addition, we have tested the dynamics using lasers with different in-plane polarizations, validating that the new vibrational mode is not dependent on the direction of the laser.

It should be noted that the lattice temperature (Figure 3c) in a laser-induced nonequilibrium system ($\tilde{T}$) is distinct from the equilibrium ionic temperature (T). $\tilde{T}$ comes from the kinetic energy of all ions defined as $\tilde{T} = Mv_{ions}^2/3k_B$, where v_{ions} is the ion velocity, M is the atomic mass, and k_B is the Boltzmann constant. The large oscillations in $\tilde{T}$ can be interpreted as that the kinetic energy and ionic potential energy exchanges coherently, while the small derivations at the later stage (e.g., at 400 K) may be due to fluctuations. Our TDDFT-MD simulations naturally include the damping of high-energy excitation, dissipated to electrons and holes at the lower levels and to the ionic subsystem as shown in Figure 3. A full equilibrium between electrons and ions is however not achievable due to the limitations of current TDDFT-MD approach.

Interestingly, the experimentally observed periodical oscillation has been successfully reproduced in our simulations (Figure 4).[8,25] The trends and features of the experimental

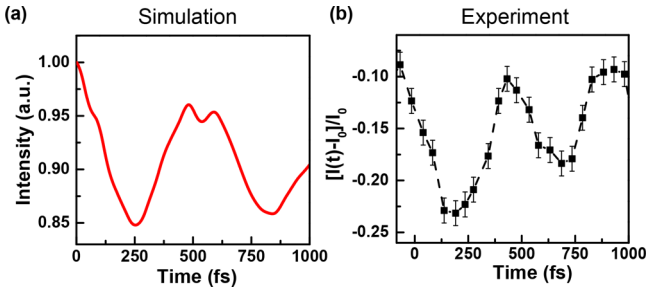

Figure 4. Simulated and experimental X-ray diffraction intensity. (a) Simulated X-ray diffraction intensity as a function of time for η = 1.92%. The RMSD is related to diffraction intensity $I(t)$ through the Debye−Waller formula, $I(t) = \exp[-Q^2\langle u^2(t)\rangle/3]$, where Q is the reciprocal lattice vector of the probed reflection, $u^2(t)$ the square of RMSD. (b) Relative change of diffracted intensity at the satellite position (1.307, 1.231, 0) as a function of pump−probe delay in bulk 1*T*-TaS_2 from ref 8.

data and our simulated X-ray diffraction intensity are almost identical, demonstrating our simulations capture the most important interactions in the experiment.[8] The calculated excitation energy E_{ex} = 0.14 eV/atom and laser fluence 0.23 mJ/cm^2 are consistent with experimental data (0.56 mJ/cm^2).[20,25] In addition, vibrational analysis shows that the photoinduced atomic displacements are quite different from that of the thermally induced phonon mode in the ground-state C phase, which has a different vibration pattern and an oscillation frequency of ∼2.3 THz (Figure S7−S9).[21,22] It is interpreted that the intriguing collective mode is attributed to the large modulation in the potential energy surface (Figure S10). As mentioned above, Eichberger et al.[21] argued that strong lasers cause the collapse of the double-well potential surface, leading to the destruction of ground-state potential and cooperative atomic motions toward the undistorted 1T phase of TaS_2. In addition, Lee and coauthors revealed that the metal−insulator transition in 1*T*-TaS_2 can be driven not by the two-dimensional orders but by the vertical stacking orders of the 2D CDWs.[39] In this study, we reveal laser excitation can greatly modify the potential energy surfaces, resulting in an intriguing collective mode with a transient metallic state.

To obtain more information about the photoexcitation induced M state (Figure 5a), we compare its structural characteristics with that of T state without any atomic distortion and the low-temperature C state. It is evident that three peaks (3.20 Å, 3.60 Å, 3.90 Å) dominate in the distribution of the Ta−Ta distances in C state (Figure 5c), while the distribution of the nearest Ta−Ta distances in the new M state (blue envelope line in the bottom of Figure 5c) exhibits only two peaks (3.36 and 3.75 Å). It should be noted that the Ta−Ta distances have the uniform value of 3.36 Å in original undistorted T state. The new emerging peak in M state around 3.75 Å is attributed to the Ta−Ta distances between

DOI: 10.1021/acs.nanolett.9b01865
Nano Lett. 2019, 19, 6027−6034

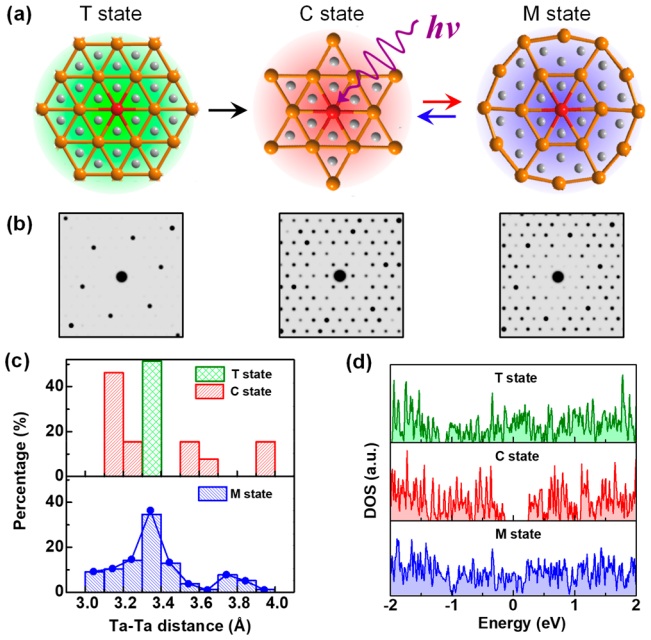

Figure 5. Atomic and electronic properties of the three states in 1*T*-TaS_2. (a) Schematic for transformation between undistorted T state (left), C state (middle) and photoinduced M state (right). (b) Simulated electron diffraction patterns for the three states. (c) Radial distribution of Ta−Ta distances in different states. The T phase is presented in green with the nearest Ta−Ta distances of 3.36 Å. (d) In-plane density of states for the three states.

the atoms in the regular central hexagons and those in the outer rings, indicating the photoinduced state is far from the T phase.

In addition to the difference in atomic structures, electron densities of states of three phases (T, C, and M) are also different as shown in Figure 5d. We obtain quite a few states around Fermi level for M phase, which is in obvious contrast with the bandgap for C state with SD. Despite both T and M states being metallic, the electronic properties are different: T state has a sharper dispersion at Fermi level compared to M state. As a result, the features in optical absorption for T and M states are also different (Figure S11). Experimentally, laser pulse with photon energy around 1.6 eV can be used to excite abundant electrons from the valence bands to conduction bands in bulk 1*T*-TaS_2 at low temperature to test our prediction, and the laser strength of E_0 = 0.04 V/Å can be easily realized.[21,56] Furthermore, the new emerging M state may be verified by electron or X-ray diffraction analysis and tested against the simulated diffraction patterns shown in Figure 5b. We emphasize that the photoexcitation-induced M state cannot be reached thermally, where the lattice displacement is at most 0.2 Å before the SD pattern melts into randomized T state at a high temperature >400 K. We note the realization of the M state could be affected by the supercell sizes and that it might disappear for larger supercells. However, it can not be explored directly due to high computational demand at this stage.

Besides the photoinduced atomic motions, useful information is also obtained from the evolution of orbital energies during the photoexcited electron−lattice dynamics (Figure S12). For a low laser intensity (η = 0.64%), the energy gap is preserved at all times, while the gap closes in a subvibrational time scale (~50 fs) for η = 1.92%, indicating the electron modulation in valence bands are suppressed and charge order unlocked to the lattice before the atomic structure responds to laser illumination. These results are in good accordance with experimental observations,[22] where not only the Mott gap at the Fermi level but also the CDW gap melts on subvibrational time scales, confirming electron−electron scatterings are at the heart of the dynamics of CDW.

The comparison between the ARPES data and the DFT results shows that the gap at Γ is obtained on a quantitative level.[49] The results naturally explain the ultrafast response of the gap observed in time-resolved ARPES experiments,[22] as the disruption and reordering of the electronic orbitals can evolve on much faster time scales than the lattice. For bulk 1*T*-TaS_2, periodic lattice distortion opens a gap (~0.45 eV, Note S2) along in-plane reciprocal vectors, resulting in a one-dimensional metal for the vertical stacking case.[49] Our calculations reveal that LDA/GGA without adding additional U describes the formation and dynamics of in-plane CDW state reasonably well. DFT calculations predicted a gap along in-plane reciprocal vectors accompanying with the one-dimensional metal,[50] while many experiments reported the Mott insulating properties in the system.[25,49] We attribute the discrepancy to the vertical orders and interlayer hybridization between different layers of 1*T*-TaS_2, which deserves further investigations.[39,49] In addition, the effect of Mott insulating nature should be paid more attention when we consider monolayer 1*T*-TaS_2 or different stacking of thin films.[57,58] For the monolayer case, we note that onsite Coulomb interactions of electrons localized within the SD cause a band separation at the Fermi level by the so-called Mott gap, with a value of 0.2 eV.[49,50]

We propose that the new intriguing collective mode can be introduced by photoexcitation, which cannot be reached by thermal phase transitions (Figure 6). The low-temperature C

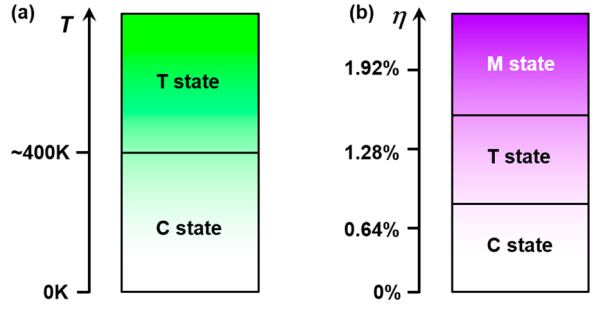

Figure 6. Schematic phase diagrams of bulk 1*T*-TaS_2. (a) Under thermal activation and (b) under different laser excitations. The C state of bulk 1*T*-TaS_2 has an equilibrium melting point at around 400 K. For η < 1.28%, bulk 1*T*-TaS_2 remains its low-temperature C state. It transforms to T state at η=1.28%. The M state emerges at higher laser intensities ($\eta \geq$ 1.92%), which is attributed to significant modifications to potential energy surface.

state melts at about 400 K due to the thermal activation, where the average equilibrium velocity of Ta is 1.4×10^{-3} Å/fs at the melting point. For the laser pulse with η = 1.28%, C state transforms to the undistorted T state, since the laser-induced velocity resulted from the changed potential energy surface is about 1.2×10^{-3} Å/fs, very close to the thermal velocity of 1.4×10^{-3} Å/fs at 400 K, resulting in a disordered distribution of Ta ions by both laser and thermal activation. However, at η > 1.92%, analysis of atomic trajectories shows that the velocities

DOI: 10.1021/acs.nanolett.9b01865
Nano Lett. 2019, 19, 6027−6034

of Ta atoms in the outer ring (4.4×10^{-3} Å/fs, the corresponding kinetic energy is 1.75×10^{-20} kg m^2 s^{-2}) are significantly larger than thermal velocities (1.4×10^{-3} Å/fs, the corresponding kinetic energy is 1.77×10^{-21} kg m^2 s^{-2}), with a highly inhomogeneous and anisotropic distribution over Ta atoms in the inner and outer rings, thanks to dramatically modified potential energy surfaces upon photoexcitation. This implies that the kinetic energies of the dynamics do not reach the thermal equilibrium distribution. The emergence of the new collective mode comes from the laser-driven dramatic changes in the interacting potential between Ta atoms. As noted, we find that upon the immediate strong excitation, the laser-induced forces on the outmost Ta in the SD is the largest (~1.4 eV/Å), while the forces acting on other Ta ions remain a relatively small value (<0.6 eV/Å). The forces are ordered and very different from the distributions in thermal equilibrium. This means that stronger laser intensities lead to specific atomic oscillation modes, which strongly suppress thermal movements of Ta and S atoms and the melting of CDW order. The transition from η = 1.28% to η = 1.92% is thus attributed to the competition between temperature-dependent thermal movements and laser-induced lattice oscillations.

To find out whether the dynamics is provoked by hot electrons or by excited electrons in nonequilibrium distribution,[20] we also performed TDDFT calculations with different initial electronic temperatures from 3000 to 5000 K with an initial ionic temperature of 10 K. For all electronic temperatures, the ionic temperatures increase at the first 100 fs and RMSD follows a similar trend (Figure S13). More importantly, there is no collapse of electronic band gap. When the excitation energy from physical photoexcitation discussed above and that from the hot electron model are compared (Table 1), it is clear

Table 1. Excitation Energy (E_{ex}, meV/Atom) for Different Laser Pulses and Electronic Temperatures (T_e) of Bulk 1*T*-TaS_2

condition	excitation energy	condition	excitation energy
η = 0.64%	40.5	T_e = 3000 K	52.3
η = 1.28%	87.5	T_e = 4000 K	92.3
η = 1.92%	141.3	T_e = 5000 K	153.8

that hot electron model requires higher energy while leading to neither melting of CDW nor the bandgap closing. This confirms that hot electron model with a well-defined electronic temperature overestimates photoexcitation energy, and electron−electron scattering is vital in the photodynamics of 1*T*-TaS_2.

The direct structural and electronic dynamic data obtained from first-principles calculations enable us to elucidate the photoinduced dynamics after optical excitations of 1*T*-TaS_2 at the atomistic spatial scale and femtosecond time scale. We also employ a larger supercell with 156 atoms (in $2\sqrt{13} \times 2\sqrt{13} \times 1$ supercell) to confirm our findings (Figure S14). We deduce that excited electrons, which do not reach an equilibrium state with a well-defined electronic temperature, play a crucial role in the dynamics of CDW state. Strong photoexcitation creates a high density of electron−hole pairs and the charge order collapses in less than 50 fs before the lattice responds, due to electron−electron scattering. Then electron−phonon interactions raise the effective lattice temperatures from 10 to 275 K in about 150 fs. Before this takes place, excited electrons strongly modulate the potential energy surface. Thus, it brings up coherent atomic motions toward a new oscillation mode with a periodicity of ~480 fs, far from thermally induced T state, which is attributed to the energy transfer between the electronic subsystem and lattice.

In conclusion, ab initio TDDFT-MD simulations reveal the nature of photoexcitation induced phase dynamics in 1*T*-TaS_2. We discover a novel collective mode induced by photodoping, which is significantly different from thermally induced phonon mode in 1*T*-TaS_2. Our results provide compelling evidence that the ultrafast dynamics in CDW state of bulk 1*T*-TaS_2 is a nonthermal process, where hot electron model is not sufficient to describe this novel phenomenon because of the lack of electron−electron scatterings. Our work provides new insights into laser-induced insulator-to-metal transition in the CDW state of 1*T*-TaS_2, and the methods adopted here might be useful for understanding a wide range of laser-modulated quantum materials.

■ ASSOCIATED CONTENT

Supporting Information

The Supporting Information is available free of charge on the ACS Publications website at DOI: 10.1021/acs.nanolett.9b01865.

Snapshots of Born−Oppenheimer MD at different temperatures, time evolution of atomic structure in 1*T*-TaS_2 under strong photoexcitation; comparison of atomic displacements between TDDFT and vibrational analysis; photoinduced atomic forces, atomic displacements from photoexcitation and thermal distortion, potential energy surface under photoexcitation, absorption spectra of three structures and TDDFT methods and parameters (PDF)

■ AUTHOR INFORMATION

Corresponding Author

*E-mail: smeng@iphy.ac.cn. Phone: +86 10 82649396.

ORCID

Jin Zhang: 0000-0001-7830-3464
Chao Lian: 0000-0002-2583-9334
Haizhong Guo: 0000-0002-6128-4225
Sheng Meng: 0000-0002-1553-1432

Author Contributions

¶J.Z., C.L., and M.G. contributed equally to this work. S.M. designed the research. Most of the calculations were performed by J.Z. and M.G. with contributions from all authors. L.C. implemented a revised version of TDDFT code. All authors contributed to the analysis and discussion of the data and the writing of the manuscript.

Notes

The authors declare no competing financial interest.

■ ACKNOWLEDGMENTS

This work was supported by National Key Research and Development Program of China (Grant Nos. 2016YFA0300902 and 2015CB921001) and National Natural Science Foundation of China (Grant Nos. 91850120 and 11774396).

■ REFERENCES

(1) Gruner, G. *Density Waves in Solids*; Perseus: Cambridge, MA, 2004.

DOI: 10.1021/acs.nanolett.9b01865
Nano Lett. 2019, 19, 6027−6034

(2) Imada, M.; Fujimori, A.; Tokura, Y. Metal-insulator transitions. *Rev. Mod. Phys.* **1998**, *70* (4), 1039.
(3) Varma, C.; Simons, A. Strong-coupling theory of charge-density-wave transitions. *Phys. Rev. Lett.* **1983**, *51* (2), 138.
(4) Liu, G.; Rumyantsev, S.; Bloodgood, M. A.; Salguero, T. T.; Balandin, A. A. Low-Frequency Current Fluctuations and Sliding of the Charge Density Waves in Two-Dimensional Materials. *Nano Lett.* **2018**, *18*, 3630−3636.
(5) Cavalieri, A. L.; Müller, N.; Uphues, T.; Yakovlev, V. S.; Baltuška, A.; Horvath, B.; Schmidt, B.; Blümel, L.; Holzwarth, R.; Hendel, S.; et al. Attosecond spectroscopy in condensed matter. *Nature* **2007**, *449* (7165), 1029−1032.
(6) Miaja-Avila, L.; Saathoff, G.; Mathias, S.; Yin, J.; Bauer, M.; Aeschlimann, M.; Murnane, M.; Kapteyn, H.; et al. Direct measurement of core-level relaxation dynamics on a surface-adsorbate system. *Phys. Rev. Lett.* **2008**, *101* (4), 046101.
(7) Schmitt, F.; Kirchmann, P. S.; Bovensiepen, U.; Moore, R. G.; Rettig, L.; Krenz, M.; Chu, J.-H.; Ru, N.; Perfetti, L.; Lu, D.; et al. Transient electronic structure and melting of a charge density wave in $TbTe_3$. *Science* **2008**, *321* (5896), 1649−1652.
(8) Laulhé, C.; Cario, L.; Corraze, B.; Janod, E.; Huber, T.; Lantz, G.; Boulfaat, S.; Ferrer, A.; Mariager, S.; Johnson, J.; et al. X-ray study of femtosecond structural dynamics in the 2D charge density wave compound 1T-TaS_2. *Phys. B* **2015**, *460*, 100−104.
(9) Ryu, H.; Chen, Y.; Kim, H.; Tsai, H.-Z.; Tang, S.; Jiang, J.; Liou, F.; Kahn, S.; Jia, C.; Omrani, A. A.; Shim, J. H.; Hussain, Z.; Shen, Z.-X.; Kim, K.; Min, B. I.; Hwang, C.; Crommie, M. F.; Mo, S.- K. Persistent Charge-Density-Wave Order in Single-Layer $TaSe_2$. *Nano Lett.* **2018**, *18*, 689−694.
(10) Hollander, M. J.; Liu, Y.; Lu, W.-J.; Li, L.-J.; Sun, Y.-P.; Robinson, J. A.; Datta, S. Electrically driven reversible insulator−metal phase transition in 1T-TaS_2. *Nano Lett.* **2015**, *15* (3), 1861−1866.
(11) Goli, P.; Khan, J.; Wickramaratne, D.; Lake, R. K.; Balandin, A. A. Charge Density Waves in Exfoliated Films of van Der Waals Materials: Evolution of Raman Spectrum in $TiSe_2$. *Nano Lett.* **2012**, *12* (11), 5941−5945.
(12) Sugawara, K.; Nakata, Y.; Shimizu, R.; Han, P.; Hitosugi, T.; Sato, T.; Takahashi, T. Unconventional charge-density-wave transition in monolayer 1T-$TiSe_2$. *ACS Nano* **2016**, *10* (1), 1341−1345.
(13) Stojchevska, L.; Vaskivskyi, I.; Mertelj, T.; Kusar, P.; Svetin, D.; Brazovskii, S.; Mihailovic, D. Ultrafast switching to a stable hidden quantum state in an electronic crystal. *Science* **2014**, *344* (6180), 177−180.
(14) Sun, H.-H.; Wang, M.-X.; Zhu, F.; Wang, G.-Y.; Ma, H.-Y.; Xu, Z.-A.; Liao, Q.; Lu, Y.; Gao, C.-L.; Li, Y.-Y.; Liu, C.; Qian, D.; Guan, D.; Jia, J.-F. Ultrathin Bismuth Film on 1T-TaS_2: Structural Transition and ChargeDensity-Wave Proximity Effect. *Nano Lett.* **2017**, *17*, 3035−3039.
(15) Laulhé, C.; Huber, T.; Lantz, G.; Ferrer, A.; Mariager, S. O.; Grübel, S.; Rittmann, J.; Johnson, J. A.; Esposito, V.; Lübcke, A.; et al. Ultrafast formation of a charge density wave state in 1T−TaS_2: Observation at nanometer scales using time-resolved X-ray diffraction. *Phys. Rev. Lett.* **2017**, *118* (24), 247401.
(16) Duong, D. L.; Ryu, G.; Hoyer, A.; Lin, C.; Burghard, M.; Kern, K. Raman Characterization of the Charge Density Wave Phase of 1T-$TiSe_2$: From Bulk to Atomically Thin Layers. *ACS Nano* **2017**, *11* (1), 1034−1040.
(17) Perfetti, L.; Loukakos, P.; Lisowski, M.; Bovensiepen, U.; Berger, H.; Biermann, S.; Cornaglia, P.; Georges, A.; Wolf, M. Time evolution of the electronic structure of 1T−TaS_2 through the insulator-metal transition. *Phys. Rev. Lett.* **2006**, *97* (6), 067402.
(18) Perfetti, L.; Loukakos, P. A.; Lisowski, M.; Bovensiepen, U.; Wolf, M.; Berger, H.; Biermann, S.; Georges, A. Femtosecond dynamics of electronic states in the Mott insulator 1T-TaS_2 by time resolved photoelectron spectroscopy. *New J. Phys.* **2008**, *10* (5), 053019.
(19) Sipos, B.; Kusmartseva, A. F.; Akrap, A.; Berger, H.; Forró, L.; Tutiš, E. From Mott state to superconductivity in 1T-TaS_2. *Nat. Mater.* **2008**, *7* (12), 960−965.
(20) Hellmann, S.; Beye, M.; Sohrt, C.; Rohwer, T.; Sorgenfrei, F.; Redlin, H.; Kalläne, M.; Marczynski-Bühlow, M.; Hennies, F.; Bauer, M.; et al. Ultrafast melting of a charge-density wave in the Mott insulator 1T−TaS_2. *Phys. Rev. Lett.* **2010**, *105* (18), 187401.
(21) Eichberger, M.; Schäfer, H.; Krumova, M.; Beyer, M.; Demsar, J.; Berger, H.; Moriena, G.; Sciaini, G.; Miller, R. D. Snapshots of cooperative atomic motions in the optical suppression of charge density waves. *Nature* **2010**, *468* (7325), 799−802.
(22) Petersen, J. C.; Kaiser, S.; Dean, N.; Simoncig, A.; Liu, H.; Cavalieri, A. L.; Cacho, C.; Turcu, I.; Springate, E.; Frassetto, F.; et al. Clocking the melting transition of charge and lattice order in 1T−TaS_2 with ultrafast extreme-ultraviolet Angle-Resolved photoemission spectroscopy. *Phys. Rev. Lett.* **2011**, *107* (17), 177402.
(23) Dean, N.; Petersen, J. C.; Fausti, D.; Tobey, R. a. I.; Kaiser, S.; Gasparov, L.; Berger, H.; Cavalleri, A. Polaronic conductivity in the photoinduced phase of 1T−TaS_2. *Phys. Rev. Lett.* **2011**, *106* (1), 016401.
(24) Ang, R.; Tanaka, Y.; Ieki, E.; Nakayama, K.; Sato, T.; Li, L.; Lu, W.; Sun, Y.; Takahashi, T. Real-Space coexistence of the melted Mott state and superconductivity in Fe-substituted 1T−TaS_2. *Phys. Rev. Lett.* **2012**, *109* (17), 176403.
(25) Hellmann, S.; Rohwer, T.; Kalläne, M.; Hanff, K.; Sohrt, C.; Stange, A.; Carr, A.; Murnane, M.; Kapteyn, H.; Kipp, L.; et al. Time-domain classification of charge-density-wave insulators. *Nat. Commun.* **2012**, *3*, 1069.
(26) Cho, D.; Cho, Y. H.; Cheong, S. W.; Kim, K. S.; Yeom, H. W. Interplay of electron-electron and electron-phonon interactions in the low-temperature phase of 1T−TaS_2. *Phys. Rev. B: Condens. Matter Mater. Phys.* **2015**, *92* (8), 085132.
(27) Ikeda, T.; Tsunetsugu, H.; Yonemitsu, K. Photoinduced Dynamics of Commensurate Charge Density Wave in 1T-TaS_2 Based on Three-Orbital Hubbard Model. *Appl. Sci.* **2019**, *9*, 70.
(28) Zong, A.; Shen, X.; Kogar, A.; Ye, L.; Marks, C.; Chowdhury, D.; Rohwer, T.; Freelon, B.; Weathersby, S.; et al. Ultrafast manipulation of mirror domain walls in a charge density wave. *Sci. Adv.* **2018**, *4*, No. eaau5501.
(29) Avigo, I.; Zhou, P.; Kalläne, M.; Rossnagel, K.; Bovensiepen, U.; Ligges, M. Excitation and Relaxation Dynamics of the Photo-Perturbed Correlated Electron System 1T-TaS_2. *Appl. Sci.* **2019**, *9*, 44.
(30) Wu, D.; Ma, Y.; Niu, Y.; Liu, Q.; Dong, T.; Zhang, S.; Niu, J.; Zhou, H.; Wei, J.; Wang, Y.; Zhao, Z.; Wang, N. Ultrabroadband photosensitivity from visible to terahertz at room temperature. *Sci. Adv.* **2018**, *4*, No. eaao3057.
(31) Wilson, J. A.; Di Salvo, F.; Mahajan, S. Charge-density waves and superlattices in the metallic layered transition metal dichalcogenides. *Adv. Phys.* **1975**, *24* (2), 117−201.
(32) Fazekas, P.; Tosatti, E. Electrical, structural and magnetic properties of pure and doped 1T-TaS_2. *Philos. Mag. B* **1979**, *39* (3), 229−244.
(33) Clerc, F.; Battaglia, C.; Bovet, M.; Despont, L.; Monney, C.; Cercellier, H.; Garnier, M.; Aebi, P.; Berger, H.; Forró, L. Lattice-distortion-enhanced electron-phonon coupling and Fermi surface nesting in 1T−TaS_2. *Phys. Rev. B: Condens. Matter Mater. Phys.* **2006**, *74* (15), 155114.
(34) Gasparov, L.; Brown, K.; Wint, A.; Tanner, D.; Berger, H.; Margaritondo, G.; Gaal, R.; Forró, L. Phonon anomaly at the charge ordering transition in 1T−TaS_2. *Phys. Rev. B: Condens. Matter Mater. Phys.* **2002**, *66* (9), 094301.
(35) Shen, W.; Ge, Y.; Liu, A. Y.; Krishnamurthy, H.; Devereaux, T.; Freericks, J. Nonequilibrium "melting" of a charge density wave insulator via an ultrafast laser pulse. *Phys. Rev. Lett.* **2014**, *112* (17), 176404.
(36) Ritschel, T.; Berger, H.; Geck, J. Stacking-driven gap formation in layered 1T-TaS_2. *Phys. Rev. B: Condens. Matter Mater. Phys.* **2018**, *98*, 195134.
(37) Lutsyk, I.; Rogala, M.; Dabrowski, P.; Krukowski, P.; Kowalczyk, P. J.; Busiakiewicz, A.; Kowalczyk, D. A.; Lacinska, E.; Binder, J.; Olszowska, N.; Kopciuszynski, M.; Szalowski, K.; Gmitra, M.; Stepniewski, R.; Jalochowski, M.; Kolodziej, J. J.; Wysmolek, A.;

DOI: 10.1021/acs.nanolett.9b01865
Nano Lett. 2019, 19, 6027−6034

Klusek, Z. Electronic structure of commensurate, nearly commensurate, and incommensurate phases of 1T−TaS_2 by angle-resolved photoelectron spectroscopy, scanning tunneling spectroscopy, and density functional theory. *Phys. Rev. B: Condens. Matter Mater. Phys.* **2018**, *98*, 195425.
(38) Skolimowski, J.; Gerasimenko, Y.; Žitko, R. Mottness collapse without metallization in the domain wall of the triangular-lattice Mott insulator 1T-TaS_2. *Phys. Rev. Lett.* **2019**, *122*, 036802.
(39) Lee, S. H.; Goh, J. S.; Cho, D. Origin of the Insulating Phase and First-Order Metal-Insulator Transition in 1T−TaS_2. *Phys. Rev. Lett.* **2019**, *122*, 106404.
(40) Shao, B.; Eich, A.; Sanders, C.; Ngankeu, A. S.; Bianchi, M.; Hofmann, P.; Khajetoorians, A. A.; Wehling, T. O. Pseudodoping of a metallic two-dimensional material by the supporting substrate. *Nat. Commun.* **2019**, *10*, 180.
(41) Runge, E.; Gross, E. K. Density-functional theory for time-dependent systems. *Phys. Rev. Lett.* **1984**, *52* (12), 997.
(42) Meng, S.; Kaxiras, E. Real-time, local basis-set implementation of time-dependent density functional theory for excited state dynamics simulations. *J. Chem. Phys.* **2008**, *129* (5), 054110.
(43) Bang, J.; Sun, Y.; Liu, X.-Q.; Gao, F.; Zhang, S. Carrier-multiplication-induced structural change during ultrafast carrier relaxation and nonthermal phase transition in semiconductors. *Phys. Rev. Lett.* **2016**, *117* (12), 126402.
(44) Lian, C.; Zhang, S.; Meng, S. Ab initio evidence for nonthermal characteristics in ultrafast laser melting. *Phys. Rev. B: Condens. Matter Mater. Phys.* **2016**, *94* (18), 184310.
(45) Ordejón, P.; Artacho, E.; Soler, J. M. Self-consistent order-N density-functional calculations for very large systems. *Phys. Rev. B: Condens. Matter Mater. Phys.* **1996**, *53* (16), R10441.
(46) Soler, J.-M.; Artacho, E.; Gale, J.-D.; García, A.; Junquera, J.; Ordejón, P.; Sánchez-Portal, D. The SIESTA method for ab initio order-N materials simulation. *J. Phys.: Condens. Matter* **2002**, *14* (11), 2745.
(47) Kolesov, G.; Grånäs, O.; Hoyt, R.; Vinichenko, D.; Kaxiras, E. Real-time TD-DFT with classical ion dynamics: methodology and applications. *J. Chem. Theory Comput.* **2016**, *12*, 122466−476.
(48) Troullier, N.; Martins, J. L. Efficient pseudopotentials for plane-wave calculations. *Phys. Rev. B: Condens. Matter Mater. Phys.* **1991**, *43* (3), 1993.
(49) Ritschel, T.; Trinckauf, J.; Koepernik, K.; Büchner, B.; Zimmermann, M. v.; Berger, H.; Joe, Y.; Abbamonte, P.; Geck, J. Orbital textures and charge density waves in transition metal dichalcogenides. *Nat. Phys.* **2015**, *11* (4), 328−331.
(50) Darancet, P.; Millis, A. J.; Marianetti, C. A. Three-dimensional metallic and two-dimensional insulating behavior in octahedral tantalum dichalcogenides. *Phys. Rev. B: Condens. Matter Mater. Phys.* **2014**, *90* (4), 045134.
(51) Vaskivskyi, I.; Gospodaric, J.; Brazovskii, S.; Svetin, D.; Sutar, P.; Goreshnik, E.; Mihailovic, I. A.; Mertelj, T.; Mihailovic, D. Controlling the metal-to-insulator relaxation of the metastable hidden quantum state in 1T-TaS_2. *Sci. Adv.* **2015**, *1* (6), No. e1500168.
(52) Cho, D.; Cheon, S.; Kim, K.-S.; Lee, S.-H.; Cho, Y.-H.; Cheong, S.-W.; Yeom, H. W. Nanoscale manipulation of the Mott insulating state coupled to charge order in 1T-TaS_2. *Nat. Commun.* **2016**, *7*, 10453.
(53) Ma, L.; Ye, C.; Yu, Y.; Lu, X.-F.; Niu, X.; Kim, S.; Feng, D.; Tománek, D.; Son, Y.-W.; Chen, X.-H.; et al. A metallic mosaic phase and the origin of Mott-insulating state in 1T-TaS_2. *Nat. Commun.* **2016**, *7*, 10956.
(54) Ligges, M.; Avigo, I.; Golež, D.; Strand, H.; Stojchevska, L.; Kalläne, M.; Rossnagel, K.; Eckstein, M.; Werner, P.; Bovensiepen, U.; et al. Ultrafast doublon dynamics in photo-excited 1T-TaS_2. *Phys. Rev. Lett.* **2018**, *120*, 166401.
(55) Han, T. R. T.; Zhou, F.; Malliakas, C. D.; Duxbury, P. M.; Mahanti, S. D.; Kanatzidis, M. G.; Ruan, C. Y. Exploration of metastability and hidden phases in correlated electron crystals visualized by femtosecond optical doping and electron crystallography. *Sci. Adv.* **2015**, *1* (5), No. e1400173.
(56) Harb, M.; Ernstorfer, R.; Hebeisen, C. T.; Sciaini, G.; Peng, W.; Dartigalongue, T.; Eriksson, M. A.; Lagally, M. G.; Kruglik, S. G.; Miller, R. D. Electronically driven structure changes of Si captured by femtosecond electron diffraction. *Phys. Rev. Lett.* **2008**, *100* (15), 155504.
(57) Yi, S.; Zhang, Z.; Cho, J.-H. Coupling between Charge, Lattice, Orbital, and Spin in a Charge Density Wave of 1T-TaS_2. *Phys. Rev. B: Condens. Matter Mater. Phys.* **2018**, *97*, No. 041413(R).
(58) Zhang, Q.; Gan, L.-Y.; Cheng, Y.; Schwingenschlögl, U. Spin polarization driven by a charge-density wave in monolayer 1T−TaS_2. *Phys. Rev. B: Condens. Matter Mater. Phys.* **2014**, *90*, No. 081103(R).

DOI: 10.1021/acs.nanolett.9b01865
Nano Lett. 2019, 19, 6027−6034